Inorg. Chem. **2008**, *47*, 4264−4274

Synthesis, Structures, and Properties of Group 9− and Group 10−Group 6 Heterodinuclear Nitrosyl Complexes

Kazuya Arashiba,[†] Hidetaka Iizuka,[†] Shoji Matsukawa,[‡] Shigeki Kuwata,[§] Yoshiaki Tanabe,[†] Masakazu Iwasaki,[¶] and Youichi Ishii*,[†]

Department of Applied Chemistry, Faculty of Science and Engineering, Chuo University, Kasuga, Bunkyo-ku, Tokyo 112-8551, Japan, Institute of Industrial Science, The University of Tokyo, Komaba, Meguro-ku, Tokyo 153-8505, Japan, Department of Applied Chemistry, Graduate School of Science and Engineering, Tokyo Institute of Technology, O-okayama, Meguro-ku, Tokyo 152-8552, Japan, and Department of Applied Chemistry, Faculty of Engineering, Saitama Institute of Technology, Okabe, Saitama 369-0293, Japan

Received November 24, 2007

The reaction of the group 9 bis(hydrosulfido) complexes $[Cp^*M(SH)_2(PMe_3)]$ (M = Rh, Ir; $Cp^* = \eta^5$-C_5Me_5) with the group 6 nitrosyl complexes $[Cp^*M'Cl_2(NO)]$ (M′ = Mo, W) in the presence of NEt_3 affords a series of bis(sulfido)-bridged early−late heterobimetallic (ELHB) complexes $[Cp^*M(PMe_3)(\mu\text{-}S)_2M'(NO)Cp^*]$ (**2a**, M = Rh, M′ = Mo; **2b**, M = Rh, M′ = W; **3a**, M = Ir, M′ = Mo; **3b**, M = Ir, M′ = W). Similar reactions of the group 10 bis(hydrosulfido) complexes $[M(SH)_2(dppe)]$ (M = Pd, Pt; dppe = $Ph_2P(CH_2)_2PPh_2$), $[Pt(SH)_2(dppp)]$ (dppp = $Ph_2P(CH_2)_3PPh_2$), and $[M(SH)_2(dpmb)]$ (dpmb = o-$C_6H_4(CH_2PPh_2)_2$) give the group 10−group 6 ELHB complexes $[(dppe)M(\mu\text{-}S)_2M'(NO)Cp^*]$ (M = Pd, Pt; M′ = Mo, W), $[(dppp)Pt(\mu\text{-}S)_2M'(NO)Cp^*]$ (**6a**, M′ = Mo; **6b**, M′ = W), and $[(dpmb)M(\mu\text{-}S)_2M'(NO)Cp^*]$ (M = Pd, Pt; M′ = Mo, W), respectively. Cyclic voltammetric measurements reveal that these ELHB complexes undergo reversible one-electron oxidation at the group 6 metal center, which is consistent with isolation of the single-electron oxidation products $[Cp^*M(PMe_3)(\mu\text{-}S)_2M'(NO)Cp^*][PF_6]$ (M = Rh, Ir; M′ = Mo, W). Upon treatment of **2b** and **3b** with ROTf (R = Me, Et; OTf = OSO_2CF_3), the O atom of the terminal nitrosyl ligand is readily alkylated to form the alkoxyimido complexes such as $[Cp^*Rh(PMe_3)(\mu\text{-}S)_2W(NOMe)Cp^*][OTf]$. In contrast, methylation of the Rh−, Ir−, and Pt−Mo complexes **2a**, **3a**, and **6a** results in S-methylation, giving the methanethiolato complexes $[Cp^*M(PMe_3)(\mu\text{-}SMe)(\mu\text{-}S)Mo(NO)Cp^*][BPh_4]$ (M = Rh, Ir) and $[(dppp)Pt(\mu\text{-}SMe)(\mu\text{-}S)Mo(NO)Cp^*][OTf]$, respectively. The Pt−W complex **6b** undergoes either S- or O-methylation to form a mixture of $[(dppp)Pt(\mu\text{-}SMe)(\mu\text{-}S)W(NO)Cp^*][OTf]$ and $[(dppp)Pt(\mu\text{-}S)_2W(NOMe)Cp^*][OTf]$. These observations indicate that O-alkylation and one-electron oxidation of the dinuclear nitrosyl complexes are facilitated by a common effect, i.e., donation of electrons from the group 9 or 10 metal center, where the group 9 metals behave as the more effective electron donor.

Introduction

Early−late heterobimetallic (ELHB) complexes in which an electron-deficient early-transition metal and an electron-rich late-transition metal are located in close proximity have recently been attracting considerable attention because the cooperative effects between such significantly different metal centers may lead to unique activation and effective transformation of substrate molecules.[1] Yet, it is little understood how early and late metals can interact in actual ELHB complexes, and obviously more information about such cooperative effects is needed to better design effective ELHB systems.[2] In the course of our study on multinuclear complexes, we have revealed that hydrosulfido complexes serve as versatile metalloligands to construct various ELHB

* To whom correspondence should be addressed. E-mail: ishii@chem.chuo-u.ac.jp.
[†] Chuo University.
[‡] The University of Tokyo.
[§] Tokyo Institute of Technology.
[¶] Saitama Institute of Technology.

(1) (a) Wheatley, N.; Kalck, P. *Chem. Rev.* **1999**, *99*, 3379–3419. (b) Stephan, D. W. *Coord. Chem. Rev.* **1989**, *95*, 41–107.

10.1021/ic702309h CCC: $40.75
Published on Web 04/22/2008

complexes.[3] In this study, we have designed group 9− and group 10−group 6 sulfido-bridged nitrosyl complexes [Cp*M(PMe$_3$)(μ-S)$_2$M′(NO)Cp*] (M = Rh, Ir; M′ = Mo, W; Cp* = η^5-C$_5$Me$_5$) and [L$_2$M(μ-S)$_2$M′(NO)Cp*] [M = Pd, Pt; M′ = Mo, W; L$_2$ = 1,2-bis(diphenylphosphino)ethane (dppe), 1,2-bis(diphenylphosphino)propane (dppp), *o*-bis(diphenylphosphinomethyl)benzene (dpmb)] and investigated the factors that control the activation of NO at the group 6 metal center.

It is well-known that the nitrosyl ligand exhibits characteristic redox behavior and reactivities depending upon the electronic states of the metal centers.[4] In particular, the terminally bound linear nitrosyl is an effective π acid and therefore is expected to be activated toward electrophilic attack, but such reactivity has poorly been exploited with actual transition-metal nitrosyl complexes.[5] On the basis of our previous results on multinuclear nitrosyl complexes,[6] we have embarked on investigating the origin of the ELHB cooperative effect in nitrosyl activation at dinuclear complexes. In this paper, we report that in the above-mentioned group 9− and group 10−group 6 dinuclear complexes the electron donation from the electron-rich late-transition (group 9 or 10) metal center plays a critical role in the activation of the nitrosyl ligand at the group 6 metal center toward electrophilic O-alkylation. Part of the results have already been published in a Communication.[7]

Experimental Section

General Remarks. All manipulations were carried out under an atmosphere of nitrogen by using standard Schlenk techniques. Dichloromethane (CH_2Cl_2) and 1,2-dichloroethane ($C_2H_4Cl_2$) were dried and distilled over P_4O_{10}, while NEt_3 was dried and distilled over KOH. The other solvents (dehydrated-grade) were purchased from Aldrich and used as received. [Cp*M(SH)$_2$(PMe$_3$)] (M = Rh, Ir),[8] [Cp*M′Cl$_2$(NO)] (**1a**, M′ = Mo; **1b**, M′ = W),[9] [M(SH)$_2$(dppe)] (M = Pd, Pt),[10] [Pt(SH)$_2$(dppp)],[11] and [MCl$_2$(dpmb)] (M = Pd, Pt)[12] were prepared according to the literature methods. ^{1}H (500 or 400 MHz) and ^{31}P{^{1}H} (202 or 121 MHz) NMR spectra were recorded on a JEOL ECA-500, JEOL JNM-GSX-400, or Varian Mercury-300 spectrometer by using $CDCl_3$ as the solvent. IR spectra were recorded on a Jasco FT/IR-410 spectrometer using KBr pellets. Elemental analyses were performed on a Perkin-Elmer 2400II CHN analyzer. Cyclic voltammetry studies were performed with a BAS CV-50W analyzer. Potentials were measured at a glassy-carbon working electrode in a CH_2Cl_2 solution containing 0.1 M (^{n}Bu$_4$N)(BF$_4$) and a 2 mM sample at 25 °C.

Preparation of [Cp*M(PMe$_3$)(μ-S)$_2$M′(NO)Cp*] (2a, M = Rh, M′ = Mo; 2b, M = Rh, M′ = W; 3a, M = Ir, M′ = Mo; 3b, M = Ir, M′ = W). The following procedure for the preparation of [Cp*Rh(PMe$_3$)(μ-S)$_2$W(NO)Cp*] (**2b**) is representative. To a solution of **1b** (475 mg, 1.13 mmol) in THF (40 mL) at −40 °C were added [Cp*Rh(SH)$_2$(PMe$_3$)] (430 mg, 1.13 mmol) and NEt_3 (0.33 mL, 2.37 mmol), and the mixture was warmed gradually to room temperature. After 3 h of stirring at room temperature, the dark-brown solution was dried up in vacuo, and the residue was dissolved in CH_2Cl_2 (15 mL) to load onto an alumina column, where the adsorbed mixture was eluted with THF−hexane (2:1). The main green band was collected, and the solvent was removed in vacuo. Recrystallization of the residual dark-green solid from benzene (20 mL)−hexane (45 mL) afforded **2b** as dark-green crystals (472 mg, 0.649 mmol, 57% yield). ^{31}P{^{1}H} NMR: δ 7.6 (d, $^1J_{RhP}$ = 147 Hz, PMe$_3$). ^{1}H NMR: δ 1.99 (s, 15H, Cp*W), 1.92 (d, $^4J_{PH}$ = 2.4 Hz, 15H, Cp*Rh), 1.25 (d, $^2J_{PH}$ = 11.0 Hz, 9H, PMe$_3$). IR (cm^{-1}): 1490 (ν_{NO}). Anal. Calcd for $C_{23}H_{39}NOPRhS_2W$: C, 37.98; H, 5.40; N, 1.93. Found: C, 38.10; H, 5.45; N, 2.00.

2a: dark-green crystals, 79% yield. ^{31}P{^{1}H} NMR: δ 11.2 (d, $^1J_{RhP}$ = 147 Hz, PMe$_3$). ^{1}H NMR: δ 1.91 (s, 15H, Cp*Mo), 1.89 (d, $^4J_{PH}$ = 2.7 Hz, 15H, Cp*Rh), 1.26 (d, $^2J_{PH}$ = 11.0 Hz, 9H, PMe$_3$). IR (cm^{-1}): 1515 (ν_{NO}). Anal. Calcd for $C_{23}H_{39}MoNOPRhS_2$: C, 43.20; H, 6.15; N, 2.19. Found: C, 43.52; H, 6.19; N, 2.27.

3a: dark-green crystals, 66% yield. ^{31}P{^{1}H} NMR: δ −22.8 (s, PMe$_3$). ^{1}H NMR: δ 1.97 (s, 15H, Cp*Mo), 1.89 (d, $^4J_{PH}$ = 1.5 Hz, 15H, Cp*Ir), 1.34 (d, $^2J_{PH}$ = 11.0 Hz, 9H, PMe$_3$). IR (cm^{-1}): 1521 (ν_{NO}). Anal. Calcd for $C_{23}H_{39}IrMoNOPS_2$: C, 37.90; H, 5.39; N, 1.92. Found: C, 38.08; H, 5.44; N, 1.97.

3b: dark-violet crystals, 48% yield. ^{31}P{^{1}H} NMR: δ −28.6 (s, PMe$_3$). ^{1}H NMR: δ 2.02 (s, 15H, Cp*W), 1.93 (d, $^4J_{PH}$ = 1.7 Hz, 15H, Cp*Ir), 1.34 (d, $^2J_{PH}$ = 11.0 Hz, 9H, PMe$_3$). IR (cm^{-1}): 1491 (ν_{NO}). Anal. Calcd for $C_{23}H_{39}IrNOPS_2W$: C, 33.82; H, 4.81; N, 1.71. Found: C, 33.68; H, 4.86; N, 1.79.

Preparation of [M(SH)$_2$(dpmb)] (M = Pd, Pt). The following procedure for the preparation of [Pt(SH)$_2$(dpmb)] is representative. A suspension of [PtCl$_2$(dpmb)] (2.79 g, 3.77 mmol) and NaSH (549

(2) (a) Kajitani, H.; Seino, H.; Mizobe, Y. *Organometallics* **2007**, *26*, 3499–3508. (b) Hernandez-Gruel, M. A. F.; Lahoz, F. J.; Dobrinovich, I. T.; Modrego, F. J.; Oro, L. A.; Pérez-Torrente, J. J. *Organometallics* **2007**, *26*, 2616–2622. (c) Takei, I.; Kobayashi, K.; Dohki, K.; Nagao, S.; Mizobe, Y.; Hidai, M. *Chem. Lett.* **2007**, *36*, 546–547. (d) Komuro, T.; Kawaguchi, H.; Lang, J.; Nagasawa, T.; Tatsumi, K. *J. Organomet. Chem.* **2007**, *692*, 1–9. (e) Herbst, K.; Söderhjelm, E.; Nordlander, E.; Dahlenburg, L.; Brorson, M. *Inorg. Chim. Acta* **2007**, *360*, 2697–2703. (f) Molina, R. H.; Kalinina, I.; Sokolov, M.; Clausen, M.; Platas, J. G.; Vicent, C.; Llusar, R. *Dalton Trans.* **2007**, 550–557. (g) Kuwabara, J.; Takeuchi, D.; Osakada, K. *Chem. Commun.* **2006**, 3815–3817. (h) Herberhold, M.; Jin, G.-X.; Rheingold, A. L. *Z. Anorg. Allg. Chem.* **2005**, *631*, 135–140. (i) Cornelissen, C.; Erker, G.; Kehr, G.; Fröhlich, R. *Organometallics* **2005**, *24*, 214–225. (j) Hidai, M.; Kuwata, S.; Mizobe, Y. *Acc. Chem. Res.* **2000**, *33*, 46–52. (k) Hanna, T. A.; Baranger, A. M.; Bergman, R. G. *J. Am. Chem. Soc.* **1995**, *117*, 11363–11364.

(3) (a) Kuwata, S.; Nagano, T.; Matsubayashi, A.; Ishii, Y.; Hidai, M. *Inorg. Chem.* **2002**, *41*, 4324–4330. For reviews of these types of synthetic methods for S-bridged complexes, see: (b) Kuwata, S.; Hidai, M. *Coord. Chem. Rev.* **2001**, *213*, 211–305. (c) Peruzzini, M.; de los Rios, I.; Romerosa, A. *Prog. Inorg. Chem.* **2001**, *49*, 169–453.

(4) (a) Hayton, T. W.; Legzdins, P.; Sharp, W. B. *Chem. Rev.* **2002**, *102*, 935–991. (b) Ford, P. C.; Lorkovic, I. M. *Chem. Rev.* **2002**, *102*, 993–1017. (c) Kuwata, S.; Kura, S.; Ikariya, T. *Polyhedron* **2007**, *26*, 4659–4663. (d) Landry, V. K.; Parkin, G. *Polyhedron* **2007**, *26*, 4751–4757. (e) Lis, E. C., Jr.; Delafuente, D. A.; Lin, Y.; Mocella, C. J.; Todd, M. A.; Liu, W.; Sabat, M.; Myers, W. H.; Harman, W. D. *Organometallics* **2006**, *25*, 5051–5058.

(5) Sharp, W. B.; Legzdins, P.; Patrick, B. O. *J. Am. Chem. Soc.* **2001**, *123*, 8143–8144.

(6) (a) Hattori, T.; Matsukawa, S.; Kuwata, S.; Ishii, Y.; Hidai, M. *Chem. Commun.* **2003**, *510*, 511. (b) Matsukawa, S.; Kuwata, S.; Hidai, M. *Inorg. Chem.* **2000**, *39*, 791–798.

(7) Arashiba, K.; Matsukawa, S.; Kuwata, S.; Tanabe, Y.; Iwasaki, M.; Ishii, Y. *Organometallics* **2006**, *25*, 560–562.

(8) (a) Klein, D. P.; Kloster, G. M.; Bergman, R. G. *J. Am. Chem. Soc.* **1990**, *112*, 2022–2024. (b) Dobbs, D. A.; Bergman, R. G. *Inorg. Chem.* **1994**, *33*, 5329–5336.

(9) Dryden, N. H.; Legzdins, P.; Batchelor, R. J.; Einstein, F. W. B. *Organometallics* **1991**, *10*, 2077–2081.

(10) (a) Schmidt, M.; Hoffmann, G. G.; Höller, R. *Inorg. Chim. Acta* **1979**, *32*, L19–L20. (b) Kato, H.; Seino, H.; Mizobe, Y.; Hidai, M. *Inorg. Chim. Acta* **2002**, *339*, 188–192.

(11) Mas-Ballesté, R.; Aullón, G.; Champkin, P. A.; Clegg, W.; Mégret, C.; González-Duarte, P.; Lledós, A. *Chem.—Eur. J.* **2003**, *9*, 5023–5035.

(12) Brown, M. D.; Levason, W.; Reid, G.; Watts, R. *Polyhedron* **2005**, *24*, 75–87.

mg, 9.79 mmol) in EtOH (70 mL) and benzene (30 mL) was refluxed for 17 h. The resulting suspension was cooled to room temperature. The precipitate was collected by filtration, washed with H_2O, EtOH, and hexane, and dried in vacuo to afford [Pt(SH)$_2$(dpmb)] as a white solid (2.23 g, 3.03 mmol, 80% yield). ^{31}P{^{1}H} NMR: δ 1.1 (s with ^{195}Pt satellites, $^1J_{PtP}$ = 2928 Hz, dpmb). ^{1}H NMR: δ 7.85−7.81, 7.48−7.41 (m, total 20H, Ph of dpmb), 7.00, 6.40 (br, 2H each, C_6H_4 of dpmb), 3.94 (d with ^{195}Pt satellites, $^2J_{PH}$ = 10.0 Hz, $^3J_{PtH}$ = 32.5 Hz, 4H, CH_2 of dpmb), −0.31 (d with ^{195}Pt satellites, $^3J_{PH}$ = 7.5 Hz, $^2J_{PtH}$ = 49.5 Hz, 2H, SH). Anal. Calcd for $C_{32}H_{30}P_2PdS_2$: C, 52.24; H, 4.11. Found: C, 51.93; H, 3.97.

[Pd(SH)$_2$(dpmb)]: yellow solid, 46% yield. ^{31}P{^{1}H} NMR: δ 11.9 (s, dpmb). ^{1}H NMR: δ 7.80−7.43 (m, 20H, Ph of dpmb), 6.99, 6.39 (br, 2H each, C_6H_4 of dpmb), 3.80 (d, $^2J_{PH}$ = 9.0 Hz, 4H, CH_2 of dpmb), −0.30 (d, $^3J_{PH}$ = 7.0 Hz, 2H, SH). Anal. Calcd for $C_{32}H_{30}P_2PdS_2$: C, 59.40; H, 4.67. Found: C, 59.18; H, 4.72.

Preparation of [(dppe)M(μ-S)$_2$M′(NO)Cp*] (4a, M = Pd, M′ = Mo; 4b, M = Pd, M′ = W; 5a, M = Pt, M′ = Mo; 5b, M = Pt, M′ = W). The following procedure for the preparation of [(dppe)Pd(μ-S)$_2$Mo(NO)Cp*] (**4a**) is representative. To a suspension of [Pd(SH)$_2$(dppe)] (355 mg, 0.62 mmol) in THF (20 mL) at −60 °C were added **1a** (206.4 mg, 0.62 mmol) in THF (20 mL) and NEt_3 (0.17 mL, 1.24 mmol), and the mixture was warmed gradually to room temperature with stirring. The dark-brown suspension was stirred overnight and then dried in vacuo. The resultant residue was dissolved in CH_2Cl_2 and loaded on an alumina column. The main brown band eluted with CH_2Cl_2−MeOH (100:2) was collected, and the volatile materials were removed in vacuo. Recrystallization of the residual dark-brown solid from CH_2Cl_2−hexane afforded **4a**·CH_2Cl_2 as brown crystals (294 mg, 0.32 mmol, 52% yield). ^{31}P{^{1}H} NMR: δ 60.3 (s, dppe). ^{1}H NMR: δ 7.78−7.41 (m, 20H, Ph of dppe), 2.45 (br, 4H, CH_2 of dppe), 1.79 (s, 15H, Cp*). IR (cm^{-1}): 1535 (ν_{NO}). Anal. Calcd for $C_{37}H_{41}Cl_2MoNOP_2PdS_2$: C, 48.56; H, 4.52; N, 1.53. Found: C, 48.62; H, 4.54; N, 1.50.

4b·$C_2H_4Cl_2$: recrystallized from $C_2H_4Cl_2$−hexane, dark-purple crystals, 63% yield. ^{31}P{^{1}H} NMR: δ 55.3 (s, dppe). ^{1}H NMR: δ 7.78−7.41 (m, 20H, Ph of dppe), 2.45 (br, 4H, CH_2 of dppe), 1.79 (s, 15H, Cp*). IR (cm^{-1}): 1499 (ν_{NO}). Anal. Calcd for $C_{38}H_{43}Cl_2NOP_2PdS_2W$: C, 44.88; H, 4.26; N, 1.38. Found: C, 44.68; H, 4.28; N, 1.36.

5a·CH_2Cl_2: eluted with CH_2Cl_2−MeOH (100:1), light-green crystals, 70% yield. ^{31}P{^{1}H} NMR: δ 50.4 (s with ^{195}Pt satellites, $^1J_{PtP}$ = 3116 Hz, dppe). ^{1}H NMR: δ 7.78−7.41 (m, 20H, Ph of dppe), 2.41 (br, 4H, CH_2 of dppe), 1.79 (s, 15H, Cp*). IR (cm^{-1}): 1534 (ν_{NO}). Anal. Calcd for $C_{37}H_{41}Cl_2MoNOP_2PtS_2$: C, 44.27; H, 4.12; N, 1.40. Found: C, 44.10; H, 4.15; N, 1.37.

5b·$C_2H_4Cl_2$: recrystallized from $C_2H_4Cl_2$−hexane, brown crystals, 46% yield. ^{31}P{^{1}H} NMR: δ 46.4 (s with ^{195}Pt satellites, $^1J_{PtP}$ = 3194 Hz, dppe). ^{1}H NMR: δ 7.76−7.43 (m, 20H, Ph of dppe), 2.45 (br, 4H, CH_2 of dppe), 1.85 (s, 15H, Cp*). IR (cm^{-1}): 1497 (ν_{NO}). Anal. Calcd for $C_{38}H_{43}Cl_2NOP_2PtS_2W$: C, 41.28; H, 3.92; N, 1.27. Found: C, 41.19; H, 3.97; N, 1.27.

Preparation of [(dppp)Pt(μ-S)$_2$M′(NO)Cp*] (6a, M′ = Mo; 6b, M′ = W). These complexes were synthesized from [Pt(SH)$_2$(dppp)] and **1a** or **1b** by a procedure similar to that described for **4a** except that CH_2Cl_2 was used as the eluent for alumina column chromatography. **6a**: green solids, 83% yield. ^{31}P{^{1}H} NMR: δ −4.0 (s with ^{195}Pt satellites, $^1J_{PtP}$ = 3056 Hz, dppp). ^{1}H NMR: δ 7.65−7.37 (m, 20H, Ph of dppp), 2.61−2.53 (br, 4H, CH_2 of dppp), 2.14−1.84 (br, 2H, CH_2 of dppp), 1.63 (s, 15H, Cp*). IR (cm^{-1}): 1535 (ν_{NO}). Anal. Calcd for $C_{37}H_{41}MoNOP_2PtS_2$: C, 47.64; H, 4.43; N, 1.50. Found: C, 47.88; H, 4.43; N, 1.45.

6b: brown solids, 56% yield. ^{31}P{^{1}H} NMR: δ −8.5 (s with ^{195}Pt satellites, $^1J_{PtP}$ = 3125 Hz, dppp). ^{1}H NMR: δ 7.63−7.35 (m, 20H, Ph of dppp), 2.66−2.51 (br, 4H, CH_2 of dppp), 2.12−1.88 (br, 2H, CH_2 of dppp), 1.78 (s, 15H, Cp*). IR (cm^{-1}): 1499 (ν_{NO}). Anal. Calcd for $C_{37}H_{41}NOP_2PtS_2W$: C, 43.54; H, 4.05; N, 1.37. Found: C, 43.65; H, 4.08; N, 1.30.

Preparation of [(dpmb)M(μ-S)$_2$M′(NO)Cp*] (7a, M = Pd, M′ = Mo; 7b, M = Pd, M′ = W; 8a, M = Pt, M′ = Mo; 8b, M = Pt, M′ = W). These complexes were obtained from [M(SH)$_2$(dpmb)] (M = Pd, Pt) by a procedure similar to that described for **4a**. **7a**·Et_2O·0.5CH_2Cl_2: eluted with CH_2Cl_2, brown crystals, 52% yield. ^{31}P{^{1}H} NMR: δ 7.8 (s, dpmb). ^{1}H NMR: δ 7.92−7.41 (m, 20H, Ph of dpmb), 6.72, 5.99 (m, 2H each, C_6H_4 of dpmb), 4.35, 3.67 (m, 2H each, CH_2 of dpmb), 1.39 (s, 15H, Cp*. IR (cm^{-1}): 1525 (ν_{NO}). Anal. Calcd for $C_{46.5}H_{54}ClMoNO_2P_2PdS_2$: C, 54.60; H, 5.32; N, 1.37. Found: C, 54.86; H, 5.31; N, 1.36.

7b·CH_2Cl_2: eluted with CH_2Cl_2−MeOH (100:2), dark-blue crystals, 76% yield. ^{31}P{^{1}H} NMR: δ 3.3 (s, dpmb). ^{1}H NMR: δ 7.94−7.40 (m, 20H, Ph of dpmb), 6.70, 5.97 (m, 2H each, C_6H_4 of dpmb), 4.32, 3.66 (m, 2H each, CH_2 of dpmb), 1.43 (s, 15H, Cp*). IR (cm^{-1}): 1482 (ν_{NO}). Anal. Calcd for $C_{43}H_{45}Cl_2NOP_2PdS_2W$: C, 47.86; H, 4.20; N, 1.30. Found: C, 47.88; H, 4.20; N, 1.30. Crystals of **7b**·MeCN suitable for X-ray analysis were obtained by further recrystallization from MeCN−Et_2O.

8a·Et_2O·0.5CH_2Cl_2: eluted with CH_2Cl_2−MeOH (100:2), green crystals, 58% yield. ^{31}P{^{1}H} NMR: δ 0.3 (s with ^{195}Pt satellites, $^1J_{PtP}$ = 3266 Hz, dpmb). ^{1}H NMR: δ 7.89−7.42 (m, 20H, Ph of dpmb), 6.74, 6.04 (m, 2H each, C_6H_4 of dpmb), 4.31, 3.91 (m, 2H each, CH_2 of dpmb), 1.42 (s, 15H, Cp*). IR (cm^{-1}): 1525 (ν_{NO}). Anal. Calcd for $C_{46.5}H_{54}ClMoNOP_2PtS_2$: C, 50.25; H, 4.90; N, 1.26. Found: C, 50.44; H, 4.97; N, 1.28.

8b·Et_2O·0.5CH_2Cl_2: eluted with CH_2Cl_2−MeOH (100:2), green crystals, 60% yield. ^{31}P{^{1}H} NMR: δ −4.1 (s with ^{195}Pt satellites, $^1J_{PtP}$ = 3332 Hz, dpmb). ^{1}H NMR: δ 7.90−7.43 (m, 20H, Ph of dpmb), 6.73, 6.02 (m, 2H each, C_6H_4 of dpmb), 4.37, 3.92 (m, 2H each, CH_2 of dpmb), 1.48 (s, 15H, Cp*). IR (cm^{-1}): 1482 (ν_{NO}). Anal. Calcd for $C_{46.5}H_{54}ClNO_2P_2PtS_2W$: C, 46.57; H, 4.54; N, 1.17. Found: C, 46.37; H, 4.45; N, 1.14.

Preparation of [Cp*M(PMe$_3$)(μ-S)$_2$M′(NO)Cp*][PF$_6$] (9a, M = Rh, M′ = Mo; 9b, M = Rh, M′ = W; 10a, M = Ir, M′ = Mo; 10b, M = Ir, M′ = W). The following procedure for the preparation of [Cp*Rh(PMe$_3$)(μ-S)$_2$W(NO)Cp*][PF$_6$] (**9b**) is representative. To a dark-green solution of **2b** (43 mg, 0.059 mmol) in CH_2Cl_2 (5 mL) was added [Cp$_2$Fe][PF$_6$] (20 mg, 0.060 mmol; Cp = η^5-C_5H_5), and the mixture was stirred at room temperature for 1 h. The resultant brown solution was filtered, and the slow addition of hexane (12 mL) to the concentrated filtrate (ca. 3 mL) afforded **9b** as dark-brown crystals (50 mg, 0.057 mmol, 97% yield). IR (cm^{-1}): 1581 (ν_{NO}). Anal. Calcd for $C_{23}H_{39}F_6NOP_2RhS_2W$: C, 31.67; H, 4.51; N, 1.61. Found: C, 31.47; H, 4.51; N, 1.62.

9a: brown solid, 81% yield. IR (cm^{-1}): 1597 (ν_{NO}). Anal. Calcd for $C_{23}H_{39}F_6MoNOP_2RhS_2$: C, 35.21; H, 5.01; N, 1.79. Found: C, 35.20; H, 4.97; N, 1.52.

10a: brown solid, 84% yield. IR (cm^{-1}): 1591 (ν_{NO}). Anal. Calcd for $C_{23}H_{39}F_6IrMoNOP_2S_2$: C, 31.61; H, 4.50; N, 1.60. Found: C, 31.75; H, 4.79; N, 1.44.

10b: dark-green crystals, 97% yield. IR (cm^{-1}): 1578 (ν_{NO}). Anal. Calcd for $C_{23}H_{39}F_6IrNOP_2S_2W$: C, 28.73; H, 4.09; N, 1.46. Found: C, 28.91; H, 4.03; N, 1.30.

Preparation of [Cp*M(PMe$_3$)(μ-S)$_2$W(NOR)Cp*][OTf] (11, M = Rh, R = Me; 12, M = Ir, R = Me; 13, M = Rh, R = Et; 14, M = Ir, R = Et). The following procedure for the preparation of [Cp*Rh(PMe$_3$)(μ-S)$_2$W(NOMe)Cp*][OTf] (**11**; OTf = OSO_2CF_3) is representative. To a dark-green solution of **2b** (160 mg, 0.220 mmol) in CH_2Cl_2 (10 mL) was added MeOTf (25 μL, 0.22 mmol) at −40 °C, and the resultant red solution was gradually warmed to room temperature. The solution was stirred overnight and dried in vacuo. The dark-red residue was recrystallized from CH_2Cl_2−hexane (5 mL−10 mL) to afford **11** as a red solid (179 mg, 0.201 mmol, 91% yield). $^{31}P\{^1H\}$ NMR: δ 8.1 (d, $^1J_{RhP}$ = 142 Hz, PMe$_3$). ^1H NMR: δ 4.06 (s, 3H, NOMe), 2.18 (s, 15H, Cp*W), 1.93 (d, $^4J_{PH}$ = 2.9 Hz, 15H, Cp*Rh), 1.31 (d, $^2J_{PH}$ = 11.2 Hz, 9H, PMe$_3$). Anal. Calcd for $C_{25}H_{42}F_3NO_4PRhS_3W$: C, 33.68; H, 4.75; N, 1.57. Found: C, 33.50; H, 4.81; N, 1.54. Single crystals of [Cp*Rh(PMe$_3$)(μ-S)$_2$W(NOMe)Cp*][PF_6] (**11′**) suitable for X-ray crystallography were obtained by the anion metathesis of **11** with $^nBu_4NPF_6$ and further recrystallization from CH_2Cl_2−hexane.

12: orange crystals, 95% yield. $^{31}P\{^1H\}$ NMR: δ −25.3 (s, PMe$_3$). ^1H NMR: δ 4.02 (s, 3H, NOMe), 2.20 (s, 15H, Cp*W), 1.94 (d, $^4J_{PH}$ = 1.2 Hz, 15H, Cp*Ir), 1.41 (d, $^2J_{PH}$ = 11.2 Hz, 9H, PMe$_3$). Anal. Calcd for $C_{25}H_{42}F_3IrNO_4PS_3W$: C, 30.61; H, 4.32; N, 1.43. Found: C, 30.37; H, 4.32; N, 1.50.

13: red crystals, 53% yield. $^{31}P\{^1H\}$ NMR: δ 9.3 (d, $^1J_{RhP}$ = 143 Hz, PMe$_3$). ^1H NMR: δ 4.27 (q, $^3J_{HH}$ = 6.4 Hz, 2H, NOCH_2CH$_3$), 2.16 (s, 15H, Cp*W), 1.92 (d, $^4J_{PH}$ = 2.7 Hz, 15H, Cp*Rh), 1.30 (m, 12H, PMe$_3$ and NOCH$_2$CH_3). Anal. Calcd for $C_{26}H_{44}F_3NO_4PRhS_3W$: C, 34.49; H, 4.90; N, 1.55. Found: C, 34.44; H, 5.01; N, 1.52.

14: brown crystals, 84% yield. $^{31}P\{^1H\}$ NMR: δ −25.5 (s, PMe$_3$). ^1H NMR: δ 4.21 (q, $^3J_{HH}$ = 7.0 Hz, 2H, NOCH_2CH$_3$), 2.16 (s, 15H, Cp*W), 1.91 (d, $^4J_{PH}$ = 1.0 Hz, 15H, Cp*Ir), 1.37 (d, $^2J_{PH}$ = 11.0 Hz, 9H, PMe$_3$), 1.26 (t, $^3J_{HH}$ = 7.0 Hz, 3H, NOCH$_2$CH_3). Anal. Calcd for $C_{26}H_{44}F_3IrNO_4PS_3W$: C, 31.39; H, 4.46; N, 1.41. Found: C, 31.00; H, 4.34; N, 1.38.

Preparation of [Cp*M(PMe$_3$)(μ-SMe)(μ-S)Mo(NO)Cp*][BPh_4] (15, M = Rh; 16, M = Ir). The following procedure for the preparation of [Cp*Rh(PMe$_3$)(μ-SMe)(μ-S)Mo(NO)Cp*][BPh_4] (**15**) is representative. To a dark-green solution of **2a** (37 mg, 0.058 mmol) in CH_2Cl_2 (5 mL) was added MeOTf (6.6 μL, 0.058 mmol) at −40 °C, and the mixture was stirred at room temperature for 5 h. The resultant dark-red solution was evaporated to dryness, and $NaBPh_4$ (ca. 20 mg) and CH_2Cl_2 (5 mL) were added to the residual solid. The mixture was filtered, and Et_2O (10 mL) was added to the concentrated filtrate (4 mL). Dark-red crystals of **15** were gradually formed upon standing at room temperature for 2 weeks, which were collected by filtration and washed with hexane (30.0 mg, 0.031 mmol, 53% yield). $^{31}P\{^1H\}$ NMR: δ 12.5 (d, $^1J_{RhP}$ = 135 Hz, PMe$_3$). ^1H NMR: δ 2.58 (s, 3H, SMe), 1.90 (s, 15H, Cp*Mo), 1.74 (d, $^4J_{PH}$ = 3.2 Hz, 15H, Cp*Rh), 0.94 (d, $^2J_{PH}$ = 11.5 Hz, 9H, PMe$_3$). IR (cm^{-1}): 1573 (ν_{NO}). Anal. Calcd for $C_{48}H_{62}BMoNOPRhS_2$: C, 59.20; H, 6.42; N, 1.44. Found: C, 59.07; H, 6.48; N, 1.39.

16: brown crystals, 54% yield. $^{31}P\{^1H\}$ NMR: δ −24.4 (s, PMe$_3$). ^1H NMR: δ 2.68 (s, 3H, SMe), 2.01 (d, $^4J_{PH}$ = 1.5 Hz, 15H, Cp*Ir), 1.93 (s, 15H, Cp*Mo), 1.36 (d, $^2J_{PH}$ = 11.5 Hz, 9H, PMe$_3$). IR (cm^{-1}): 1572 (ν_{NO}). Anal. Calcd for $C_{48}H_{62}BIrMoNOPS_2$: C, 54.23; H, 5.88; N, 1.32. Found: C, 54.20; H, 6.24; N, 1.20.

Preparation of [(dppp)Pt(μ-SMe)(μ-S)Mo(NO)Cp*][OTf]·CH_2Cl_2 (17·CH_2Cl_2). MeOTf (8.0 mg, 0.049 mmol) was added to a solution of **6a** (42.0 mg, 0.045 mmol) in CH_2Cl_2 (5 mL) at −60 °C. The mixture was stirred overnight at room temperature, and then the volatiles were removed in vacuo. The brown residue was recrystallized from CH_2Cl_2−hexane to afford **17**·CH_2Cl_2 as orange crystals (40.0 mg, 0.034 mmol, 75%). $^{31}P\{^1H\}$ NMR: δ −9.1 (d with ^{195}Pt satellites, J_{PP} = 32 Hz, $^1J_{PtP}$ = 3054 Hz, dppp), −13.6 (d with ^{195}Pt satellites, J_{PP} = 32 Hz, $^1J_{PtP}$ = 2884 Hz, dppp). ^1H NMR: δ 7.68−7.29 (m, 20H, Ph of dppp), 3.53−3.45, 3.29−3.22 (m, 1H each, CH_2 of dppp), 2.90−2.81 (m, 2H, CH_2 of dppp), 2.63−2.50 (br, 2H, CH_2 of dppp), 2.22 (d with ^{195}Pt satellites, $^4J_{PH}$ = 3.5 Hz, $^3J_{PtH}$ = 34.0 Hz, 3H, SMe), 1.76 (s, 15H, Cp*). IR (cm^{-1}): 1603 (ν_{NO}). Anal. Calcd for $C_{40}H_{46}Cl_2F_3MoNO_4P_2PtS_3$: C, 40.65; H, 3.92; N, 1.19. Found: C, 40.51; H, 3.87; N, 1.13.

Reaction of 6b with MeOTf. MeOTf (1 equiv) was added to a solution of **6b** in CH_2Cl_2 at −60 °C to afford a mixture of the S-methylated complex [(dppp)Pt(μ-SMe)(μ-S)W(NO)Cp*](OTf) (**18**) and the O-methylated complex [(dppp)Pt(μ-S)$_2$W(NOMe)-Cp*](OTf) (**19**) (ca. 2:1, determined by $^{31}P\{^1H\}$ and ^1H NMR). These complexes could not be separated but were characterized spectroscopically.

18. $^{31}P\{^1H\}$ NMR: δ −9.4 (d with ^{195}Pt satellites, J_{PP} = 30 Hz, $^1J_{PtP}$ = 3098 Hz, dppp), −13.8 (d with ^{195}Pt satellites, J_{PP} = 30 Hz, $^1J_{PtP}$ = 2970 Hz, dppp). ^1H NMR: δ 2.36 (br, 3H, SMe), 1.86 (s, 15H, Cp*). IR (cm^{-1}): 1602 (ν_{NO}).

19. $^{31}P\{^1H\}$ NMR: δ −8.9 (s with ^{195}Pt satellites, $^1J_{PtP}$ = 3088 Hz, dppp). ^1H NMR: δ 3.77 (s, 3H, NOMe), 1.93 (s, 15H, Cp*).

Preparation of [Cp*M(PMe$_3$)(μ-S)$_2$W(O)Cp*](OTf) (20, M = Rh; 21, M = Ir). The following procedure for the preparation of [Cp*Rh(PMe$_3$)(μ-S)$_2$W(O)Cp*][OTf] (**20**) is representative. To a dark-green solution of **2b** (53.0 mg, 0.073 mmol) in CH_2Cl_2 (5 mL) was added HOTf (13 μL, 0.15 mmol) at −40 °C, and the resultant red solution was gradually warmed to room temperature. The solution was stirred overnight and was dried in vacuo. The residual red oil was recrystallized from CH_2Cl_2 (2 mL)−Et_2O (20 mL) to afford **20** as orange needles (47.3 mg, 0.055 mmol, 75% yield). $^{31}P\{^1H\}$ NMR: δ 8.7 (d, $^1J_{RhP}$ = 140 Hz, PMe$_3$). ^1H NMR: δ 2.22 (s, 15H, Cp*W), 2.00 (d, $^4J_{PH}$ = 2.5 Hz, 15H, Cp*Rh), 1.39 (d, $^2J_{PH}$ = 11.5 Hz, 9H, PMe$_3$). IR (cm^{-1}): 909 ($\nu_{W=O}$). Anal. Calcd for $C_{24}H_{39}F_3O_4PRhS_3W$: C, 33.42; H, 4.56. Found: C, 33.40; H, 4.60. Single crystals of [Cp*Rh(PMe$_3$)(μ-S)$_2$W(O)Cp*][BPh_4] (**20′**) suitable for X-ray crystallography were obtained by the anion metathesis of **20** with $NaBPh_4$ and further recrystallization from CH_2Cl_2−Et_2O.

21: yellow needles, 51% yield. $^{31}P\{^1H\}$ NMR: δ −22.7 (s, PMe$_3$). ^1H NMR: δ 2.23 (s, 15H, Cp*W), 2.02 (d, $^4J_{PH}$ = 1.5 Hz, 15H, Cp*Ir), 1.46 (d, $^2J_{PH}$ = 11.5 Hz, 9H, PMe$_3$). IR (cm^{-1}): 910 ($\nu_{W=O}$). Anal. Calcd for $C_{24}H_{39}F_3IrO_4PS_3W$: C, 30.29; H, 4.13. Found: C, 30.13; H, 4.02.

Magnetic Moment Measurements. The ambient-temperature solution magnetic moment of **9b** was measured by the Evans method.[13] A CD_2Cl_2 solution of **9b** with known concentration (6.8 mM) was prepared and placed in an NMR tube. A ^1H NMR spectrum was first recorded, and then a coaxial reference capillary filled with pure CD_2Cl_2 was inserted inside the sample tube. A second ^1H NMR spectrum, which clearly showed the original and the paramagnetically shifted deuterated solvent peaks, was thus obtained. The magnetic moment was calculated using equations and parameters cited in ref 14.

X-ray Diffraction Studies. Diffraction data for **2b**, **4a**·CH_2Cl_2, **9b**, **11′**, **15**, and **20′** were collected on a Rigaku AFC-7S four-

(13) Evans, D. F. *J. Chem. Soc.* **1959**, 2003–2005.
(14) (a) Chufán, E. E.; Verani, C. N.; Puiu, S. C.; Rentschler, E.; Schatzschneider, U.; Incarvito, C.; Rheingold, A. L.; Karlin, K. D. *Inorg. Chem.* **2007**, *46*, 3017–3026. (b) O'Connor, C. J. *Progress in Inorganic Chemistry*; John Wiley & Sons Inc.: New York, 1982; Vol. *29*; pp 203−283. (c) Lide, D. R., Ed. *CRC Handbook of Chemistry and Physics*, 86th ed.; CRC Press: Boca Raton, FL, 2005.

Table 1. X-ray Crystallographic Data for **2b**, **4a**·CH_2Cl_2, **6a**, and **7b**·MeCN

	2b	**4a**·CH_2Cl_2	**6a**	**7b**·MeCN
chemical formula	$C_{23}H_{39}NOPRhS_2W$	$C_{37}H_{41}Cl_2MoNOP_2PdS_2$	$C_{37}H_{41}MoNOP_2PtS_2$	$C_{44}H_{46}N_2OP_2PdS_2W$
fw	727.42	915.05	932.83	1035.18
dimens of crystals	0.60 × 0.30 × 0.30	0.50 × 0.30 × 0.30	0.20 × 0.20 × 0.20	0.20 × 0.20 × 0.20
cryst syst	monoclinic	monoclinic	orthorhombic	orthorhombic
space group	$P2_1/n$	$P2_1/n$	*Pbca*	*Pnma*
a, Å	17.008(2)	22.457(4)	18.643(4)	19.175(4)
b, Å	18.843(2)	15.578(5)	15.995(3)	17.553(4)
c, Å	17.127(2)	23.520(5)	23.338(5)	12.300(3)
α, deg				
β, deg	97.121(8)	105.15(2)		
γ, deg				
V, Å^3	5446(1)	7942(3)	6959(3)	4140(2)
Z	8	8	8	4
ρ_{calcd}, g cm^{-3}	1.774	1.530	1.781	1.661
F(000)	2864	3696	3680	2056
μ, cm^{-1}	50.57	11.180	46.030	34.287
transmn factor range	0.164−0.219	0.546−0.715	0.261−0.398	0.388−0.504
2θ range, deg	5−55	5−55	5−55	5−55
no. of reflns measd	13 308	18 718	47 349	29 676
no. of unique reflns	12 486	18 261	7986	4897
no. of reflns used [$I > 3\sigma(I)$]	8566	7227	2413	2993
no. of param refined	620	930	447	281
R [$I > 3\sigma(I)$][a]	0.037	0.048	0.035	0.021
R_w [$I > 3\sigma(I)$][b]	0.038	0.050	0.035	0.025
GOF [$I > 3\sigma(I)$][c]	1.012	1.001	1.004	1.004
max diff peak/hole, e Å^{-3}	+0.81/−1.60	+0.48/−0.44	+1.90/−0.81	+1.54/−0.61

[a] $R = \sum||F_o| - |F_c||/\sum|F_o|$. [b] $R_w = [\sum w(|F_o| - |F_c|)^2/\sum wF_o^2]^{1/2}$, $w = [pF_o^2 + q\sigma(F_o^2) + r]^{-1}$ [$p = 0.0001$ (**2b** and **6a**), 0.0003 (**4a**·CH_2Cl_2), 0 (**7b**·MeCN); $q = 1.2$ (**2b**), 1.55 (**4a**·CH_2Cl_2), 0.55 (**6a**), 0.35 (**7b**·MeCN); $r = 0.25$ (**2b**), 0 (**4a**·CH_2Cl_2, **6a**, and **7b**·MeCN)]. [c] GOF = $[\sum w(|F_o| - |F_c|)^2/(N_{obs} - N_{params})]^{1/2}$.

circle automated diffractometer (crystal-to-detector distance 235 mm) with graphite-monochromated Mo Kα radiation ($\lambda = 0.710\,69$ Å) at room temperature using the $\omega-2\theta$ scan technique. Diffraction data for **6a** and **7b**·MeCN were collected on a Rigaku Mercury CCD area detector (crystal-to-detector distance 45 mm) with graphite-monochromated Mo Kα radiation ($\lambda = 0.710\,69$ Å) at −150 °C. Cell parameters were determined by least-squares refinement of 25 machine-centered reflections for **2b**, **4a**·CH_2Cl_2, **9b**, **11′**, **15**, and **20′** or of reflections among $5 < 2\theta < 55°$ for **6a** and **7b**·MeCN. Intensity data were corrected for empirical absorptions (Ψ scans for **2b**, **4a**·CH_2Cl_2, **9b**, **11′**, **15**, and **20′**; REQAB for **6a** and **7b**·MeCN) and for Lorentz−polarization effects.[15] A correction for secondary extinction was further applied for **2b** [coefficient, 32(5)], **4a**·CH_2Cl_2 [coefficient, 57(8)], **9b** [coefficient, 35(4)], **11′** [coefficient, 52(2)], and **20′** [coefficient, 16(2)].[16] No significant decay was observed during the collection of reflections. The structure solution and refinements were carried out using the *CrystalStructure* crystallographic software package.[17] The positions of the heavy atoms were determined by direct methods (*SIR92* for **7b**·MeCN; *SHELX97* for **20′**)[18] or by Patterson methods (*PATTY* for **2b**, **4a**·CH_2Cl_2, **9b**, **11′**, and **15**; *SHELX-97* for **6a**),[19] and the remaining non-H atoms were found by subsequent Fourier syntheses.[20] All non-H atoms were refined on F_o [$I > 3\sigma(I)$] anisotropically by full-matrix least-squares techniques, while all the H atoms were placed at calculated positions with fixed isotropic parameters. The atomic scattering factors were taken from ref 21. Anomalous dispersion effects were included in F_c.[22] The values of $\Delta f'$ and $\Delta f''$ were taken from ref 23. Details of the X-ray diffraction study are summarized in Tables 1 and 2.

Results and Discussion

Synthesis and Structure of Group 9−Group 6 Heterodinuclear Complexes 2 and 3. When the bis(hydrosulfido) complexes of the group 9 metals [Cp*M$(SH)_2(PMe_3)$] (M = Rh, Ir) were allowed to react with an equimolar amount of the group 6 nitrosyl complexes [Cp*M′Cl_2(NO)] (**1**) in the presence of 2 equiv of NEt_3, the bis(sulfido)-bridged ELHB complexes [Cp*M$(PMe_3)(\mu$-S$)_2$M′(NO)Cp*] (**2** and **3**) were obtained in good-to-moderate yields (eq 1). The molybdenum complexes **2a** and **3a** show one strong IR

(15) Jacobson, R. A. *REQAB: private communication to Rigaku Corp.*; Rigaku Corp.: Tokyo, Japan, 1998.

(16) Larson, A. C. In *Crystallographic Computing: Proceedings of an International Summer School Organized by The Commission on Crystallographic Computing of the International Union of Crystallography and Held in Ottawa, August 4−11, 1969*; Ahmed, F. R., Hall, S. R., Huber, C. P., Eds.; Munksgaard: Copenhagen, Denmark, 1970; pp 291–294.

(17) (a) *CrystalStructure 3.60: Single Crystal Structure Analysis Software*; Rigaku Corp.: The Woodlands, TX, 2000–2004. (b) Watkin, D. J.; Prout, C. K.; Carruthers, J. R.; Betteridge, P. W. *CRYSTALS Issue 10*; Chemical Crystallography Laboratory: Oxford, U.K., 1996.

(18) (a) Altomare, A.; Cascarano, G.; Giacovazzo, C.; Guagliardi, A.; Burla, M. C.; Polidori, G.; Camalli, M. *J. Appl. Crystallogr.* **1994**, *27*, 435. (b) Altomare, A.; Burla, M. C.; Camalli, M.; Cascarano, G. L.; Giacovazzo, C.; Guagliardi, A.; Moliterni, A. G. G.; Polidori, G.; Spagna, R. *J. Appl. Crystallogr.* **1999**, *32*, 115–119. (c) Sheldrick, G. M. *SHELX-97: Program for the Refinement of Crystal Structure*; University of Göttingen: Göttingen, Germany, 1997.

(19) Beurskens, P. T.; Admiraal, G.; Behm, H.; Beurskens, G.; Bosman, W. P.; García-Granda, S.; Gould, R. O.; Smits, J. M. M.; Smykalla, C. *Z. Kristallogr., Suppl.* **1991**, *4*, 99.

(20) Beurskens, P. T.; Beurskens, G.; de Gelder. R.; García-Granda, S.; Gould, R. O.; Israël, R.; Smits, J. M. M. *The DIRDIF-99 program system*; Crystallography Laboratory, University of Nijmegen: Nijmegen, The Netherlands, 1999.

(21) Cromer, D. T.; Waber, J. T. In *International Tables for X-ray Crystallography*; Ibers, J. A., Hamilton, W. C., Eds.; Kynoch Press: Birmingham, England, 1974; Vol. *IV*, Table 2.2 A.

(22) Ibers, J. A.; Hamilton, W. C. *Acta Crystallogr.* **1964**, *17*, 781–782.

(23) (a) Creagh, D. C.; Hubbell, J. H. In *International Tables for X-ray Crystallography*; Wilson, A. J. C., Ed.; Kluwer Academic Publishers: Boston, MA, 1992; Vol. *C*, Table 4.2.4.3. (b) Creagh, D. C.; McAuley, W. J. In *International Tables for X-ray Crystallography*; Wilson, A. J. C., Ed.; Kluwer Academic Publishers; Boston, MA, 1992; Vol. *C*, Table 4.2.6.8.

Table 2. X-ray Crystallographic Data for **9b**, **11′**, **15**, and **20′**

	9b	**11′**	**15**	**20′**
chemical formula	$C_{23}H_{39}F_6NOP_2RhS_2W$	$C_{24}H_{42}F_6NOP_2RhS_2W$	$C_{48}H_{62}BMoNOPRhS_2$	$C_{47}H_{59}BOPRhS_2W$
fw	872.38	887.42	973.77	1032.64
dimens of crystals	0.50 × 0.40 × 0.30	0.90 × 0.30 × 0.20	0.40 × 0.40 × 0.20	1.00 × 0.30 × 0.30
cryst syst	orthorhombic	monoclinic	triclinic	triclinic
space group	*Pbcn*	$P2_1/c$	$P\bar{1}$	$P\bar{1}$
a, Å	17.627(2)	8.714(3)	10.204(1)	12.236(1)
b, Å	16.322(2)	24.849(4)	18.072(3)	17.377(2)
c, Å	21.780(2)	14.533(2)	27.000(5)	11.669(1)
α, deg			75.05(1)	103.311(8)
β, deg		91.52(2)	88.46(1)	94.657(8)
γ, deg			82.92(1)	73.725(8)
V, Å^3	6266(1)	3145(1)	4773(1)	2317.3(4)
Z	8	4	4	2
ρ_{calcd}, g cm^{-3}	1.849	1.874	1.355	1.480
F(000)	3416	1744	2016	1040
μ, cm^{-1}	44.87	44.71	7.62	29.953
transmn factor range	0.209−0.260	0.176−0.409	0.702−0.859	0.315−0.407
2θ range, deg	5−55	5−55	5−55	5−55
no. of reflns measd	7890	7875	22 495	11 100
no. of unique reflns	7201	7213	21 897	10 603
no. of reflns used [$I > 3\sigma(I)$]	4151	6041	8584	8546
no. of param refined	376	422	1133	547
R [$I > 3\sigma(I)$][a]	0.036	0.030	0.053	0.031
R_w [$I > 3\sigma(I)$][b]	0.038	0.031	0.054	0.032
GOF [$I > 3\ \sigma(I)$][c]	1.008	1.018	1.014	1.014
max diff peak/hole, e Å^{-3}	+0.90/−0.52	+1.12/−1.26	+0.60/−0.62	+1.61/−1.33

[a] $R = \sum||F_o| - |F_c||/\sum|F_o|$. [b] $R_w = [\sum w(|F_o| - |F_c|)^2/\sum wF_o^2]^{1/2}$, $w = [pF_o^2 + q\sigma(F_o^2) + r]^{-1}$ [$p = 0.0002$ (**9b**), 0.0001 (**11′**, **15**, and **20′**); $q = 1.0$ (**9b**), 3.0 (**11′**), 1.1 (**15**), 1.8 (**20′**); $r = 0.15$ (**9b**), 0.10 (**11′** and **15**), 0.30 (**20′**)]. [c] GOF = $[\sum w(|F_o| - |F_c|)^2/(N_{obs} - N_{params})]^{1/2}$.

absorption assignable to the NO stretching around 1520 cm^{-1} and the tungsten congeners **2b** and **3b** at 1490 cm^{-1}. These ν(NO) values are among the lowest for linear nitrosyl complexes and suggest the existence of strong M′→NO back-bonding.[24] Particularly noteworthy is the large red shift from the mononuclear thiolato complexes [Cp*M′(NO)(SPh)$_2$] [ν(NO) = 1631 (M′ = Mo), 1609 (M′ = W) cm^{-1}],[25] which mimic the coordination environment of **2** and **3** except for the neighboring rhodium or iridium center. We thus attribute the strong π back-bonding primarily to the influx of electrons from the group 9 metal center through the M^{III} →M′^{II} dative bond.[26] The ^{1}H NMR spectra display a set of signals due to two distinct Cp* ligands and one PMe_3 ligand, being well in accordance with the formulation.

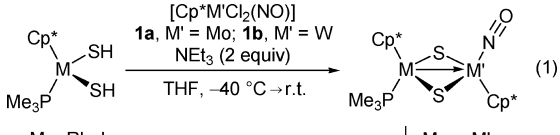

(1)

	M	M'
2a	Rh	Mo
2b	Rh	W
3a	Ir	Mo
3b	Ir	W

The molecular structure of **2b** has been established by an X-ray diffraction study (Table 3). The unit cell contains two independent but very similar complex molecules, one of which is shown in Figure 1. Both rhodium and tungsten centers adopt a three-legged piano-stool geometry. The two Cp* ligands occupy mutually trans positions with respect to the $RhWS_2$ ring. Within the $RhWS_2$ core, the short Rh−W distance (2.91 Å, mean) as well as the acute Rh−S−W angles (75.9°, mean) clearly indicates the presence of a dative bond from Rh^{III} to W^{II} in agreement with the 34e structure

Table 3. Selected Bond Lengths (Å) and Angles (deg) for **2b**

molecule 1		molecule 2	
W1−Rh1	2.9149(6)	W2−Rh2	2.8986(6)
W1−S1	2.331(2)	W2−S3	2.342(2)
W1−S2	2.327(2)	W2−S4	2.330(2)
W1−N1	1.754(6)	W2−N2	1.746(6)
W1−C1	2.337(7)	W2−C24	2.338(8)
W1−C2	2.355(8)	W2−C25	2.353(8)
W1−C3	2.538(8)	W2−C26	2.525(8)
W1−C4	2.551(8)	W2−C27	2.531(8)
W1−C5	2.375(7)	W2−C28	2.343(8)
Rh1−S1	2.390(2)	Rh2−S3	2.396(2)
Rh1−S2	2.394(2)	Rh2−S4	2.385(2)
N1−O1	1.244(9)	N2−O2	1.255(9)
W1−S1−Rh1	76.25(6)	W2−S3−Rh2	75.44(6)
W1−S2−Rh1	76.24(6)	W2−S4−Rh2	75.86(6)
W1−N1−O1	169.8(5)	W2−N2−O2	170.1(5)

of **2b**. As mentioned above, this electron donation between the metal atoms is responsible for the electron-rich nature of the W^{II} center. Enhancement of the π donation of the bridging S atoms by the Rh atom is not evident, because the

(24) (a) Hayton, T. W.; Legzdins, P.; Patrick, B. O. *Inorg. Chem.* **2002**, *41*, 5388–5396. (b) Müller, A.; Eltzner, W.; Clegg, W.; Sheldrick, G. M. *Angew. Chem., Int. Ed. Engl.* **1982**, *21*, 536–537. (c) Chen, Z.; Schmalle, H. W.; Fox, T.; Berke, H. *Dalton Trans.* **2005**, 580–587.

(25) Jin, G.-X.; Herberhold, M. *Transition Met. Chem.* **2001**, *26*, 445–447.

(26) In complexes **2** and **3**, the π donation from the S atoms to the molybdenum/tungsten center is considered to be stronger than that in [Cp*M′(NO)(SPh)$_2$] (M′ = Mo, W) because of the four-electron repulsion from the 18e rhodium/iridium center, and this effect may also be responsible to the low ν_{NO} values of **2** and **3** (see ref 27). However, as described below, the W−S bond distances in **2b** are not as exceptional as 16e W^{II}−S bonds. Therefore, we believe that the Rh/Ir → Mo/W dative bond plays the major role in the increase of the electron density at the Mo/W center.

(27) (a) Fox, D. C.; Fiedler, A. T.; Halfen, H. L.; Brunold, T. C.; Halfen, J. A. *J. Am. Chem. Soc.* **2004**, *126*, 7627–7638. (b) Galindo, A.; Mealli, C.; Cuyás, J.; Miguel, D.; Riera, V.; Pérez-Martínez, J. A.; Bois, C.; Jeannin, Y. *Organometallics* **1996**, *15*, 2735–2744.

W−S distances in **2b** (2.33 Å) are comparable with those in the related mononuclear polysulfido complex [Cp*W(NO)(S_5)] (2.33 Å).[28] It should also be mentioned that the two W−C bonds trans to the nitrosyl ligand (2.53−2.55 Å) are meaningfully longer than the other three W−C bonds (2.34−2.37 Å), although the Cp* protons are indistinguishable in the ^{1}H NMR spectrum even at −90 °C. We consider that the increased electron density of the tungsten center, in combination with the trans influence of the nitrosyl ligand,[29] causes the displacement of the Cp* ligand on the W atom from the symmetrical η^5-coordination.[30] Despite the electron richness of the tungsten center and the consequent strong π back-donation, the structure of the W−N−O moiety is not exceptional as a linear nitrosyl ligand.

Synthesis and Structure of Group 10−Group 6 Heterodinuclear Complexes 4−8. When the group 10 bis(hydrosulfido) complexes [L_2M($SH)_2$] (L_2 = dppe, dppp, dpmb; M = Pd, Pt) were used as templates to react with **1**, a series of group 10−group 6 ELHB complexes [(dppe)M(μ-$S)_2$M′(NO)Cp*] (**4** and **5**), [(dppp)Pt(μ-$S)_2$M′(NO)Cp*] (**6**), and [(dpmb)M(μ-$S)_2$M′(NO)Cp*] (**7** and **8**) were obtained in good-to-moderate yields (eq 2). In the IR spectra, an NO stretching is observed at around 1530 cm^{-1} for the molybdenum complexes **4a**−**8a** and 1500 cm^{-1} for the tungsten complexes **4b**−**8b**. The lowest ν_{NO} values are observed for M(dpmb)−W complexes **7b** and **8b** at around 1480 cm^{-1} (overlapping with a ν_{PPh} band). The ^{1}H and ^{31}P{^{1}H} NMR spectra of **4**−**8** are consistent with the formulation and indicative of a C_s symmetrical structure.

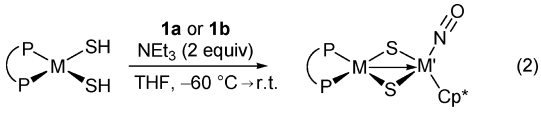

M = Pd, Pt

P P = dppe, dppp, dpmb

	M	M'	P P
4a	Pd	Mo	dppe
4b	Pd	W	dppe
5a	Pt	Mo	dppe
5b	Pt	W	dppe
6a	Pt	Mo	dppp
6b	Pt	W	dppp
7a	Pd	Mo	dpmb
7b	Pd	W	dpmb
8a	Pt	Mo	dpmb
8b	Pt	W	dpmb

The detailed molecular structure of **4a** has been determined by X-ray crystallography (Figure 2 and Table 4). The unit cell contains two crystallographically independent molecules, but their structures are essentially the same. The Pd atom has a square-planar geometry, and the $PdMoS_2$ core is slightly puckered where the dihedral angle between the PdS_2 and MoS_2 planes is 165.3°. On the other hand, the structure of the molybdenum center is closely related to that of the tungsten center in **2b** except that the displacement of the Cp* ligand from η^5 coordination is not as remarkable as that in **2b**. The separation of Pd−Mo (2.91 Å, mean) and the acute angle of Pd−S−Mo (76.9°, mean) suggest the presence of a dative bond from Pd^{II} to Mo^{II}.

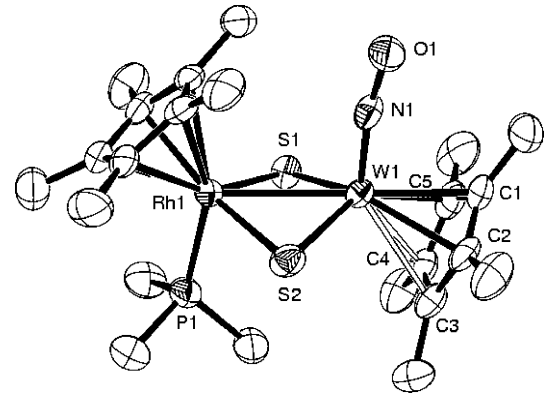

Figure 1. Molecular structure of **2b**. One of the two crystallographically independent components in the crystal is shown. Thermal ellipsoids are shown at the 50% probability level. H atoms are omitted for clarity.

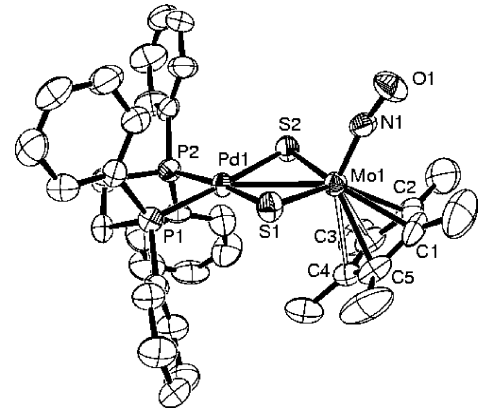

Figure 2. Molecular structure of **4a**·CH_2Cl_2. One of the two crystallographically independent molecules in the crystal is shown. Thermal ellipsoids are shown at the 50% probability level. H atoms are omitted for clarity.

Table 4. Selected Bond Lengths (Å) and Angles (deg) for **4a**·CH_2Cl_2

molecule 1		molecule 2	
Mo1−Pd1	2.9142(10)	Mo2−Pd2	2.9149(10)
Mo1−S1	2.335(2)	Mo2−S3	2.327(2)
Mo1−S2	2.327(2)	Mo2−S4	2.329(2)
Mo1−N1	1.772(7)	Mo2−N2	1.761(7)
Mo1−C1	2.311(12)	Mo2−C38	2.320(11)
Mo1−C2	2.341(10)	Mo2−C39	2.391(12)
Mo1−C3	2.457(9)	Mo2−C40	2.475(10)
Mo1−C4	2.470(9)	Mo2−C41	2.466(9)
Mo1−C5	2.403(11)	Mo2−C42	2.328(9)
Pd1−S1	2.364(2)	Pd2−S3	2.355(2)
Pd1−S2	2.364(2)	Pd2−S4	2.353(2)
N1−O1	1.223(9)	N2−O2	1.228(9)
Mo1−S1−Pd1	76.65(8)	Mo2−S3−Pd2	77.01(8)
Mo1−S2−Pd1	76.81(8)	Mo2−S4−Pd2	77.01(8)
Mo1−N1−O1	170.1(7)	Mo2−N2−O2	169.5(7)
P1−Pd1−P2	86.15(9)	P3−Pd2−P4	85.76(9)
P1−Pd1−S1	84.82(9)	P3−Pd2−S3	88.01(9)
P2−Pd1−S2	87.79(9)	P4−Pd2−S4	84.54(9)
S1−Pd1−S2	101.24(9)	S3−Pd2−S4	101.69(9)

(28) Herberhold, M.; Jin, G.-X.; Kremnitz, W.; Rheingold, A. L.; Haggerty, B. S. *Z. Naturforsch. B: Chem. Sci.* **1991**, *46b*, 500–506.

(29) Gomez-Sal, P.; de Jesús, E.; Michiels, W.; Royo, P.; Vázque de Miguel, A.; Martínez-Carrera, S. *J. Chem. Soc., Dalton Trans.* **1990**, 2445–2449.

(30) (a) The electron-rich metal centers in the formally 20e complexes [Cp_2Mo(NO)Me] and [Cp^*_2Mo(N)(N_3)] are known to reduce the hapticity of the Cp ligands to a greater extent. Cotton, F. A.; Rusholme, G. A. *J. Am. Chem. Soc.* **1972**, *94*, 402–406. (b) Shin, J. H.; Bridgewater, B. M.; Churchill, D. G.; Baik, M.-H.; Friesner, R. A.; Parkin, G. *J. Am. Chem. Soc.* **2001**, *123*, 10111–10112.

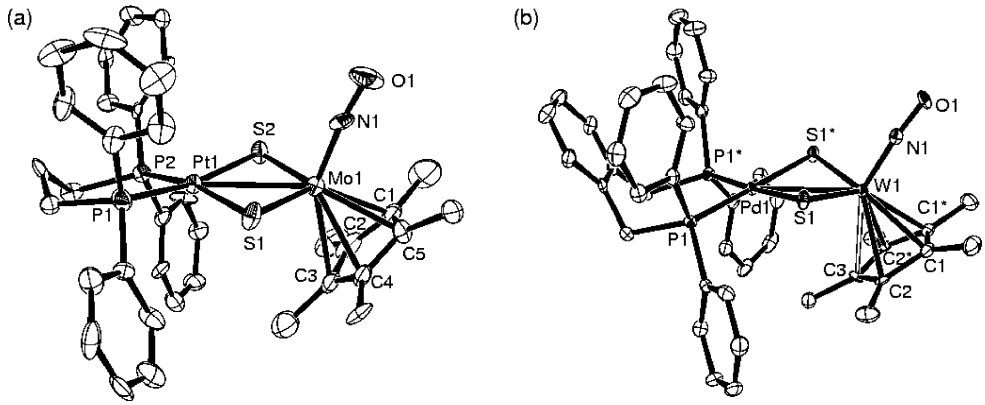

Figure 3. Molecular structures of **6a** (a) and **7b**·MeCN (b). Thermal ellipsoids are shown at the 50% probability level. H atoms are omitted for clarity.

Table 5. Selected Bond Lengths (Å) and Angles (deg) for **6a** and **7b**·MeCN

6a		**7b**·MeCN	
Mo1−Pt1	2.9189(12)	W1−Pd1	2.9565(5)
Mo1−S1	2.329(3)	W1−S1	2.3101(10)
Mo1−S2	2.317(3)	W1−N1	1.763(4)
Mo1−N1	1.764(11)	W1−C1	2.339(3)
Mo1−C1	2.467(15)	W1−C2	2.441(4)
Mo1−C2	2.417(13)	W1−C3	2.483(5)
Mo1−C3	2.331(13)	Pd1−S1	2.3833(11)
Mo1−C4	2.309(14)	N1−O1	1.244(6)
Mo1−C5	2.432(15)		
Pt1−S1	2.377(3)		
Pt1−S2	2.365(3)		
N1−O1	1.226(15)		
Mo1−S1−Pt1	76.66(10)	W1−S1−Pd1	78.07(3)
Mo1−S2−Pt1	77.13(10)	W1−N1−O1	174.9(4)
Mo1−N1−O1	172.5(9)	P1−Pd1−P1*	103.24(4)
P1−Pt1−P2	98.55(13)	S1−Pd1−S1*	96.77(4)
		P1−Pd1−S1	79.95(3)

The molecular structures of (dppp)Pt−Mo complex **6a** and (dpmb)Pd−W complex **7b** were also confirmed by crystallographic studies (Figure 3 and Table 5). Complex **7b** has a crystallographic mirror plane containing the Pd1, W1, N1, O1, and C3 atoms. The total coordination geometries of **6a** and **7b** are similar to that of **4a**, but the difference in the phosphine chelate ring size gives rise to the slight deformation of the core structure. Unlike **4a**, the $PtMoS_2$ atoms in **6a** are almost coplanar, while the P_2S_2 coordination arrangement around the platinum center is distorted from planarity, where the PtP_2 plane is skewed by 13.9° from the PtS_2 plane. On the other hand, the palladium center in **7b** adopts almost a planar geometry, while the $PdWS_2$ core is considerably puckered (159.1°). In all cases, the nitrosyl ligands keep the linear coordination mode.

Electrochemical Properties of 2−8. The electron-rich nature of the group 6 metal centers in **2**−**8** was further demonstrated by cyclic voltammetry measurements. As shown in Table 6, complexes **2**−**8** undergo reversible single-electron oxidations. The dinuclear complexes containing molybdenum are oxidized at 0.22−0.24 V (for the group 9 metal complexes) or 0.37−0.41 V (for the group 10 metal complexes) vs SCE and those containing tungsten at 0.12−0.13 V (for the group 9 metal complexes) or 0.29−0.31 V (for the group 10 metal complexes). Because the potentials are governed by the group 6 metals regardless of the group 9 and 10 metals, the oxidation could be ascribed mainly to that of the group 6 metal center. The chelate size of the diphosphine in complexes **4**−**8** has little effect on the oxidation potentials. No notable reduction waves are observed in the range down to −1.5 V. These results make a sharp contrast with the redox behavior of the parent mononuclear group 6 nitrosyl complexes [Cp*M′X_2(NO)] (M′ = Mo, X = Cl, Br, I; M′ = W, X = I), for which a reversible single-electron reduction at −0.3 to −0.5 V has been reported.[31] In the present ELHB complexes, the flux of electrons from the neighboring late metal center obviously increases the electron density at the group 6 metal center and facilitates its oxidation. It is also interesting to note that the group 9−group 6 complexes **2** and **3** are oxidized at lower potentials by about 0.17 V than the group 10−group 6 complexes **4**−**8** in spite of the lower oxidation state of the group 10 metals. We consider that the formal 18e structure of the Rh^{III}/Ir^{III} center in **2** and **3** contributes to the more effective electron donation than the formal 16e Pd^{II}/Pt^{II} center in **4**−**8**.

Table 6. Cyclic Voltammetry Data for the Oxidation Potentials of Complexes **2**−**8**

compound	$E_{1/2}$[a]	$i_{p,c}/i_{p,a}$
2a	+0.24	1.27
3a	+0.22	1.18
4a	+0.39	0.69
5a	+0.39	0.92
6a	+0.37	0.94
7a	+0.41	0.73
8a	+0.41	0.81
2b	+0.13	1.30
3b	+0.12	0.94
4b	+0.32	0.92
5b	+0.31	0.99
6b	+0.30	0.96
7b	+0.29	0.91
8b	+0.31	1.01

[a] vs SCE, reversible.

One-Electron Oxidation of 2 and 3. On the basis of the electrochemical behavior of **2**−**8**, we next examined isolation of the one-electron-oxidation products. Treatment of **2** and **3** with [Cp_2Fe][PF_6] afforded the cationic complexes [Cp*M-(PMe_3)(μ-S)$_2$M′(NO)Cp*][PF_6] (**9** and **10**) in excellent yield (eq 3). Extremely broadened ^{1}H NMR spectra clearly indicate the paramagnetic nature of **9** and **10**. Complex **9b** exhibits

(31) Herring, F. G.; Legzdins, P.; Richter-Addo, G. B. *Organometallics* **1989**, *8*, 1485–1493.

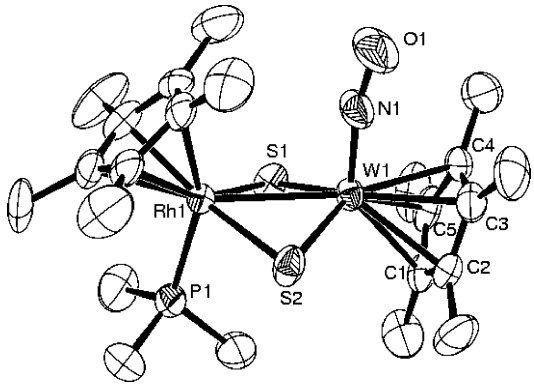

Figure 4. Molecular structure of the cationic part of **9b**. Thermal ellipsoids are shown at the 50% probability level. H atoms are omitted for clarity.

Table 7. Selected Bond Lengths (Å) and Angles (deg) for **9b**

W1−Rh1	2.8833(6)	W1−C3	2.358(8)
W1−S1	2.2780(19)	W1−C4	2.364(8)
W1−S2	2.284(2)	W1−C5	2.368(7)
W1−N1	1.796(7)	Rh1−S1	2.370(2)
W1−C1	2.404(7)	Rh1−S2	2.383(2)
W1−C2	2.384(7)	N1−O1	1.222(10)
W1−S1−Rh1	76.66(6)	W1−N1−O1	167.4(6)
W1−S2−Rh1	76.28(6)		

$\mu_{eff} = 1.87$ (Evans NMR method), which is consistent with an $S = {}^1/_2$ system. In good agreement with the oxidation of the group 6 metal center, **9** and **10** exhibit an NO stretching band at around 1595 cm^{-1} (molybdenum complexes) or 1580 cm^{-1} (tungsten complexes), which is about 100 cm^{-1} blue-shifted compared to those for **2** and **3**. The molecular structure of **9b** was fully established by an X-ray analysis (Figure 4 and Table 7). The Rh−W [2.8833(6) Å] and W−S (2.28 Å, mean) bond distances are slightly shorter than those of **2b**, suggesting oxidation of the tungsten center. On the other hand, the Cp* ligand at the tungsten center adopts a normal η^5-coordination mode with the approximately equivalent W−C distances (2.36−2.40 Å), which is also consistent with the lower electron density at the W atom than in **2b**. In contrast to **2** and **3**, oxidation of **4**−**8** with $[Cp_2Fe][PF_6]$ resulted in unidentified complex mixtures.

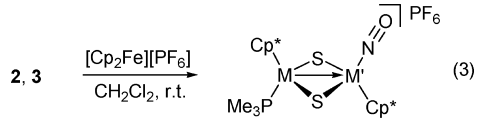

(3)

	M	M'
9a	Rh	Mo
9b	Rh	W
10a	Ir	Mo
10b	Ir	W

Alkylation of Complexes 2 and 3. As described above, complexes **2**−**8** are featured by the strong π back-bonding to the nitrosyl ligand. We have therefore examined their reactivities with electrophiles. As expected, treatment of the M−W complex **2b** or **3b** with 1 equiv of ROTf (R = Me, Et; OTf = OSO_2CF_3) in CH_2Cl_2 selectively afforded the M^{III}/W^{VI} alkoxyimido complexes $[Cp^*M(PMe_3)(\mu\text{-}S)_2W(NOR)Cp^*](OTf)$ (**11**−**14**) through the electrophilic O-alkylation of the nitrosyl ligand (eq 4). These complexes have been

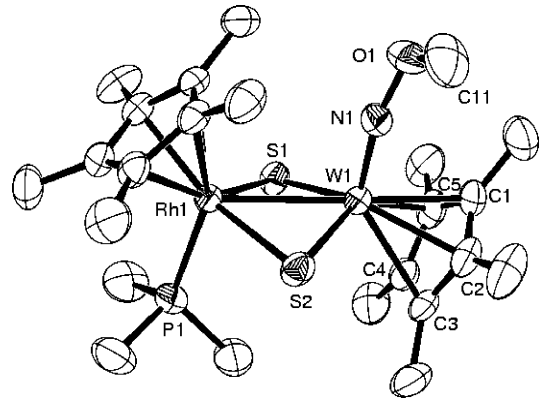

Figure 5. Molecular structure of the cationic part of **11′**. Thermal ellipsoids are shown at the 50% probability level. H atoms are omitted for clarity. Selected bond lengths (Å) and angles (deg): W1−Rh1 2.9096(3), W1−S1 2.297(1), W1−S2 2.303(1), W1−N1 1.747(4), Rh1−S1 2.388(1), Rh1−S2 2.398(1), N1−O1 1.350(6), O1−C11 1.436(7), W1−S1−Rh1 76.74(4), W1−S2−Rh1 76.46(4), W1−N1−O1 164.0(3), N1−O1−C11 112.3(4).

characterized by the absence of IR absorptions ascribable to the NO multiple bond and a new ^{1}H NMR resonance for the alkoxy group. The detailed structure of $[Cp^*Rh(PMe_3)(\mu\text{-}S)_2W(NOMe)Cp^*](PF_6)$ (**11′**), which is obtained by the anion metathesis of **11** with $[Bu_4N][PF_6]$, has been unambiguously determined by an X-ray crystallographic study (Figure 5). The W−N−O moiety is essentially linear [164.0(3)°], being diagnostic of the four-electron donor character of the alkoxyimido ligand. The metrical parameters of the alkoxyimido ligand in **11′** are comparable to those in $[CpNbCl_2(NOBu^t)]$, which was derived from an O-*tert*-butylhydroxylamine salt.[32] It should be mentioned that electrophilic methylation of a genuine terminal nitrosyl ligand has not been described in the literature. The closest example to the present reaction is the methylation of the anionic nitrosyl complex $[Cp^*MoMe_3(NO)Li(thf)_2]_2$, giving the methoxyimido complex $[Cp^*MoMe_3(NOMe)]$.[33] The Mo−N−O−Li array in the former lithiated complex, however, has been revealed to be a bridging oxoimido ligand on the basis of X-ray crystallography [Mo−N, 1.742(2) Å; N−O, 1.279(3) Å] and IR spectroscopy ($\nu_{NO} = 1399$ cm^{-1}). On the other hand, the μ-NO ligands are known to be more activated toward electrophilic attack, and several examples of their methylation have been documented.[34]

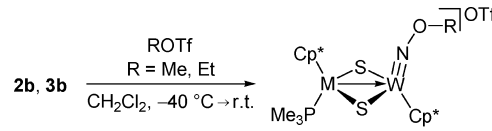

(4)

	M	R
11	Rh	Me
12	Ir	Me
13	Rh	Et
14	Ir	Et

In contrast to the O-alkylation of **2b** and **3b**, treatment of the M−Mo complexes **2a** and **3a** with MeOTf followed by

(32) Green, M. L. H.; James, J. T.; Sanders, J. F. *Chem. Commun.* **1996**, 1343–1344.
(33) Sharp, W. B.; Daff, P. J.; McNeil, W. S.; Legzdins, P. *J. Am. Chem. Soc.* **2001**, *123*, 6272–6282.

Scheme 1

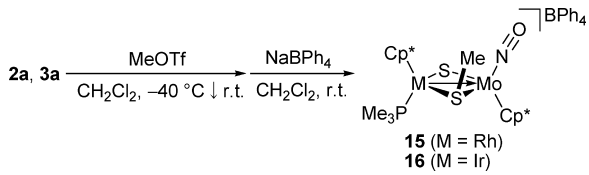

the anion metathesis with $NaBPh_4$ resulted in selective formation of the methanethiolato complexes [Cp*M(PMe_3)(μ-SMe)(μ-S)Mo(NO)Cp*][BPh_4] (**15** and **16**; Scheme 1).[35] Complex **15** exhibits a ν_{NO} band at 1573 cm^{-1} in the IR spectrum and a singlet at δ 2.58 attributable to an SMe group. The former value is about 60 cm^{-1} blue-shifted in the reaction, reflecting the cationic nature of the $RhMoS_2$ core. The S-methylation structure of **15** has further been confirmed by X-ray analysis (Figure 6 and Table 8). The total coordination geometry of **15** is comparable to that of **2b** except for the S−Me group, but it should be noted that the Mo−SMe distance is considerably longer (ca. 0.07 Å) than the Mo−S(sulfido) distance, while the Rh−SMe and Rh−S(sulfido) distances are nearly the same. The SMe group is syn to the nitrosyl ligand, probably to avoid the steric repulsion with the PMe_3 ligand. Judging from the results of the alkylation of **2** and **3**, π back-donation from the more electron-rich tungsten center is necessary for sufficient activation of NO toward O-alkylation. This tendency parallels well with the ν_{NO} values and the oxidation potentials of **2** and **3**.

Methylation of Pt−M′ Complexes 6. Analogously to the methylation of **2a** and **3a**, the reaction of Pt−Mo complex **6a** with 1 equiv of MeOTf yielded the S-methylated complex [(dppp)Pt(μ-SMe)(μ-S)Mo(NO)Cp*][OTf] (**17**) in 75% yield (eq 5).[36] Complex **17** shows two doublets at δ −9.1 and −13.6 with ^{195}Pt satellites in the $^{31}P\{^1H\}$ NMR spectrum as well as one doublet ($^4J_{PH}$ = 3.5 Hz) with ^{195}Pt satellites at δ 2.22 due to the SMe protons in the ^{1}H NMR, indicating the methylation of one of the bridging sulfur ligands. On the other hand, a similar reaction of Pt−W complex **6b** led to a mixture of the S-methylated complex [(dppp)Pt(μ-SMe)(μ-S)W(NO)-Cp*][OTf] (**18**) and the O-methylated complex [(dppp)Pt(μ-S)$_2$W(NOMe)Cp*][OTf] (**19**) in a ratio of 2:1 (determined by NMR spectra; eq 6).[35] Complex **18** has been unambiguously characterized by the $^{31}P\{^1H\}$ NMR resonances at δ −9.4 and −13.8 (d with ^{195}Pt satellites), the ^{1}H NMR signal at δ 2.36 (br, SMe), and the IR absorption at 1602 cm^{-1} (ν_{NO}) and **19** by the characteristic methoxyimido signal at δ 3.77 (s) in the ^{1}H NMR spectrum. These observations indicate that the group 10−group 6 complexes possess a lower tendency to undergo the O-alkylation of the nitrosyl ligand than the group 9−group 6 complexes, which is in full agreement with the results of the IR and cyclic voltammetry measurements. Thus, not only the tungsten center, which forms effective π back-bonding, but also the late metal center, which boosts the π-electron donation through the metal−metal bond, are essential for the O-alkylation of the ELHB nitrosyl complexes.

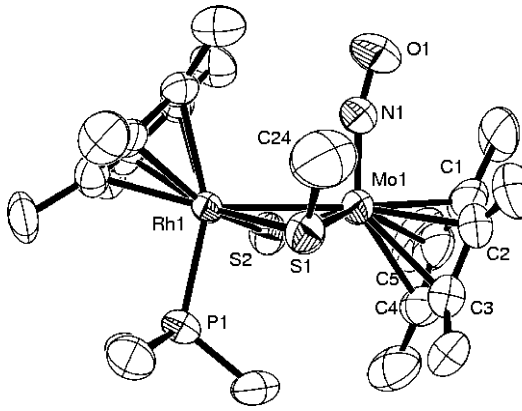

Figure 6. Molecular structure of the cationic part of **15**. One of the two crystallographically independent components in the crystal is shown. Thermal ellipsoids are shown at the 50% probability level. Hydrogen atoms are omitted for clarity.

Table 8. Selected Bond Lengths (Å) and Angles (deg) for **15**

molecule 1		molecule 2	
Mo1−Rh1	2.940(1)	Mo2−Rh2	2.940(1)
Mo1−S1	2.385(3)	Mo2−S3	2.391(2)
Mo1−S2	2.317(3)	Mo2−S4	2.324(3)
Mo1−N1	1.76(1)	Mo2−N2	1.758(8)
Rh1−S1	2.395(3)	Rh2−S3	2.389(2)
Rh1−S2	2.400(3)	Rh2−S4	2.413(2)
N1−O1	1.22(1)	N2−O2	1.21(1)
Mo1−S1−Rh1	75.92(9)	Mo2−S3−Rh2	75.92(6)
Mo1−S2−Rh1	77.10(9)	Mo2−S4−Rh2	76.71(7)
Mo1−N1−O1	164.9(9)	Mo2−N2−O2	167.4(9)

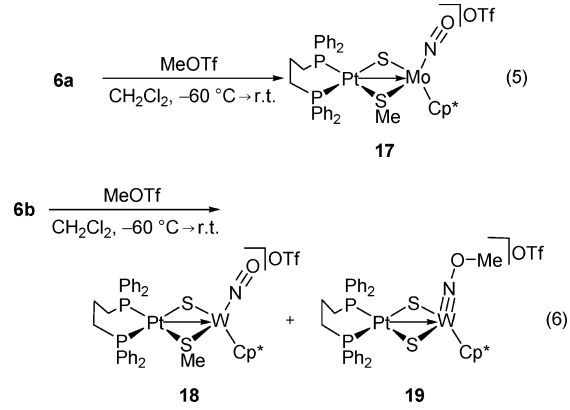

Reaction of 2b and 3b with HOTf. In addition to the alkylation reactions, protonation of the ELHB complexes has been attempted as an electrophilic functionalization of the nitrosyl ligand. With respect to the protonation of a terminal

(34) (a) Stevens, R. E.; Gladfelter, W. L. *J. Am. Chem. Soc.* **1982**, *104*, 6454–6457. (b) Stevens, R. E.; Guettler, R. D.; Gladfelter, W. L. *Inorg. Chem.* **1990**, *29*, 451–456. (c) Barr, M. E.; Bjarnason, A.; Dahl, L. F. *Organometallics* **1994**, *13*, 1981–1991. (d) Lee, K. K. H.; Wong, W. T. *J. Chem. Soc., Dalton Trans.* **1996**, 1707–1720.

(35) No thermal interconversion between **15** and Rh–Mo analog of **11** or **18** and **19** has been observed. The S-methylated complexes **15** and **18** decompose at 70 °C in $C_2H_4Cl_2$ without formation of the O-methylated complexes, while **11** and **19** are stable at this temperature.

(36) (a) For S-alkylation of [Pt_2(diphosphine)$_2$(μ-S)$_2$] complexes, see: Chong, S. H.; Henderson, W.; Hor, T. S. A. *Dalton Trans.* **2007**, 4008–4016. (b) Nova, A.; González-Duarte, P.; Lledós, A.; Mas-Ballesté, R.; Ujaque, G. *Inorg. Chim. Acta* **2006**, *359*, 3763–3744, and references cited therein.

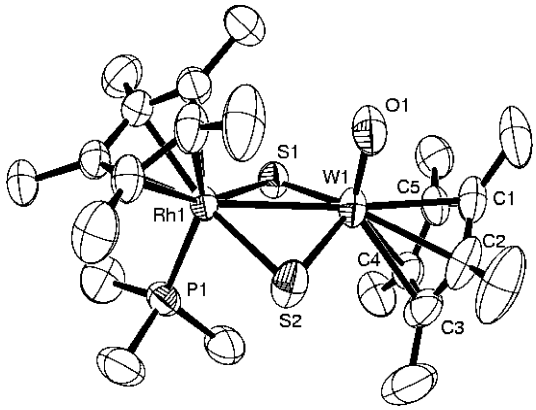

Figure 7. Molecular structure of the cationic part of **20′**. Thermal ellipsoids are shown at the 50% probability level. H atoms are omitted for clarity. Selected bond lengths (Å) and angles (deg): W1−Rh1 2.8635(4), W1−S1 2.2555(10), W1−S2 2.2700(12), W1−O1 1.723(2), Rh1−S1 2.3884(10), Rh1−S2 2.3866(14), W1−S1−Rh1 76.08(2), W1−S2−Rh1 75.85(3).

nitrosyl ligand, N-protonation has mainly been reported for late-transition-metal nitrosyls,[37] whereas O-protonation of a (nitrosyl)tungsten complex has only recently been described by Legzdins and co-workers.[5,38]

Treatment of **2b** and **3b** with excess HOTf (2 equiv) gave the cationic oxo complexes [Cp*M(PMe_3)(μ-S)$_2$W(O)Cp*][OTf] (**20** and **21**; eq 7). Complexes **20** and **21** were characterized by NMR, IR, and elemental analyses, and the detailed structure was confirmed by X-ray analysis of [Cp*Rh(PMe_3)(μ-S)$_2$W(O)Cp*][BPh_4] (**20′**), which is obtained by the anion metathesis of **20** with $NaBPh_4$ (Figure 7). The W−O [1.723(2) Å] and W−S [2.2555(10) and 2.2700(12) Å] distances are similar to those of [Cp*W(O)(μ-S)$_2$Ru(CH_3CN)(PPh_3)$_2$][OTf] [W−O 1.727(3) Å, W−S 2.26 Å, mean).[39] From the analogy to the alkylation, we presume that the first step of the above reaction is the O-protonation of the nitrosyl ligand. Subsequent hydrolysis would lead to complex **20**, but unfortunately nitrogenous products could not be identified. We must await further investigation to reveal the mechanism for this reaction.

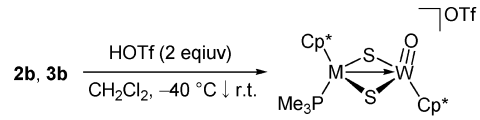

(7)

20 (M = Rh)
21 (M = Ir)

Conclusion

We have synthesized a series of bis(sulfido)-bridged ELHB complexes composed of a group 6 metal nitrosyl as the reaction site and a group 9 or group 10 metal fragment as the electron pool and demonstrated that the latter unit increases the electron density on the former through the metal−metal dative bond. The 18e group 9 M^{III} center (Cp*M(PMe_3)(μ-S)$_2$) is shown to work as a more efficient electron donor than the 16e group 10 M^{II} center ((diphosphine)M(μ-S)$_2$). Treatment of the Rh/Ir−W complexes **2b** and **3b** with ROTf results in the electrophilic O-alkylation of the terminal nitrosyl ligand owing to the enormous π back-donation to the nitrosyl ligand assisted by donation from the late metal center in the ELHB core. In contrast, S-methylation takes place for the ELHB complexes with less electron-rich nitrosyl ligands. Further studies on the electrophilic functionalization of nitrosyl and related ligands at the ELHB complexes are currently underway.

Acknowledgment. Financial support by the Ministry of Education, Culture, Sports, Science and Technology of Japan and Chuo University (Joint Research Grant) is appreciated.

Supporting Information Available: Crystallographic data for **2b**, **4a**·CH_2Cl_2, **6a**, **7b**·MeCN, **9b**, **11′**, **15**, and **20′** in CIF format. This material is available free of charge via the Internet at http://pubs.acs.org.

IC702309H

(37) (a) Farmer, P. J.; Sulc, F. *J. Inorg. Biochem.* **2005**, *99*, 166–184. (b) Melenkivitz, R.; Hillhouse, G. L. *Chem. Commun.* **2002**, 660–661.
(38) Obayashi, E.; Takahashi, S.; Shiro, Y. *J. Am. Chem. Soc.* **1998**, *120*, 12964–12965.
(39) Ohki, Y.; Matsuura, N.; Marumoto, T.; Kawaguchi, H.; Tatsumi, K. *J. Am. Chem. Soc.* **2003**, *125*, 7978–7988.